DOE/NASA/51044-21
NASA TM-82667



# Results of the ETV-1 Breadboard Tests Under Steady-State and Transient Conditions

Noel B. Sargent and Miles O. Dustin
National Aeronautics and Space Administration
Lewis Research Center



Work performed for
**U.S. DEPARTMENT OF ENERGY**
**Conservation and Renewable Energy**
**Office of Vehicle and Engine R&D**

Prepared for
Electric Vehicle Council Symposium VI
Baltimore, Maryland, October 21-23, 1981

## NOTICE

DOE/NASA/51044-21
NASA TM-82667

# Results of the ETV-1 Breadboard Tests Under Steady-State and Transient Conditions

Noel B. Sargent and Miles O. Dustin
National Aeronautics and Space Administration
Lewis Research Center
Cleveland, Ohio 44135

Work performed for
U.S. DEPARTMENT OF ENERGY
Conservation and Renewable Energy
Office of Vehicle and Engine R&D
Washington, D.C. 20545
Under Interagency Agreement DE-AI01-77CS51044

Prepared for
Electric Vehicle Council Symposium VI
Baltimore, Maryland, October 21-23, 1981

# RESULTS OF THE ETV-1 BREADBOARD TESTS UNDER STEADY-STATE AND TRANSIENT CONDITIONS

by Noel B. Sargent and Miles O. Dustin

National Aeronautics and Space Administration
Lewis Research Center
Cleveland, Ohio 44135

## ABSTRACT

This paper presents the test results of a breadboard version of the ETV-1 electric vehicle propulsion system built by General Electric Company under contract to NASA-LeRC as a part of the Department of Energy (DOE) Electric and Hybrid Vehicle Program. The breadboard was installed in the NASA-LeRC Road Load Simulator facility and tested under steady state and transient conditions. Steady state tests were run to characterize the system and component efficiencies over the complete speed-torque capabilities of the propulsion system in both motoring and regenerative modes of operation. The steady state data were obtained using a battery simulator to separate the effects on efficiency caused by changing battery state-of-charge and component temperature. Transient tests were performed to determine the energy profiles of the propulsion system operating over the SAE J227a driving schedules.

E-944

## BACKGROUND

The NASA-LeRC under the direction of DOE is responsible for the test and evaluation of electric and hybrid vehicle propulsion systems and components. In September 1978 a contracted effort was undertaken to design, fabricate, and deliver a propulsion system breadboard of the Electric Test Vehicle-1 (ETV-1) vehicle. The ETV-1 propulsion system was developed for DOE by the General Electric Corporation and the Chrysler Corporation. It was chosen for test because it is a good example of the state of the art of dc electric propulsion systems in terms of design and system integration. The ETV-1 propulsion system (Ref. 1) utilizes a 108-volt battery pack, transistorized armature and field choppers, a shunt-wound dc motor, and a transaxle, consisting of a single speed, two-stage speed reducer-differential. The ETV-1 propulsion system was provided to NASA-LeRC by GE in a breadboard configuration. The breadboard contains a complete set of duplicate vehicle propulsion system components on a test frame while maintaining the components in their in-vehicle configuration as nearly as possible. The breadboard configuration is shown on Fig. 1 and a description of the ETV-1 components given in Table 1. A torque-speed transducer was inserted between the motor and transaxle snafts. The insertion of this transducer required the physical separation of the motor flange from the transaxle and the addition of a single support bearing at the transaxle input. Electric power leads were increased in length as required to install current shunts. Sufficient instrumentation was provided to separately measure the efficiency of each individual component. Testing began in Marcn 1980 on a temporary dynamometer and later continued on the Road Load Simulator (RLS). Testing on the RLS was conducted from August 1980 to February 1981.

### Facility Description

Road load simulator. The RLS is a specialized laboratory dynamometer facility specifically designed to dynamically reproduce vehicle conditions encountered on the road (Ref. 2). These loads or road torques are applied directly to the test propulsion system output axle shaft. These torques are the sum of the tire losses, aerodynamic drag, road grade and inertial effects as represented by the equation

$$T_{net} = K_1 + K_2 v + K_3 v^2 + K_4 \frac{dv}{dt} + K_5 \sin \theta,$$

where $T_{net}$ is the net torque, $v$ is the vehicle velocity, $\theta$ is the road grade angle, $K_1$ and $K_2$ relate to tire friction, $K_3$ to aerodynamic drag, $K_4$ to inertial torque and $K_5$ to road grade.

Once determined for a particular vehicle, these K vales are used as inputs to the automatic torque control of the RLS. For dynamic tests, speed control is provided by a special interface which utilizes a preprogrammed command speed vs. time profile (the "D" cycle for example) and the speed feedback from the RLS to execute accelerator and brake commands as required to match the preprogrammed profile (Ref. 2).

For steady state test, both speed and torque are selected and controlled. The RLS is operated in the speed control mode and once set the propulsion system speed is maintained by the RLS at the selected setting. The torque value is then adjusted using the propulsion system accelerator for

positive torques and the brake for negative torques.

Battery simulator. Initial testing with batteries revealed a significant change in system efficiency over the course of a long-term test due to the combined effects of state-of-charge variation (which changes battery voltage) and component temperature variation. For this reason a battery simulator was used to stabilize voltage for most steady state tests. The battery simulator is composed of a motor-generator set and a capacitor bank (Ref. 2).

Instrumentation. The breadboard was instrumented to isolate the efficiency of each component in the propulsion system. This was accomplished by measuring the appropriate current-voltage pairs with wide-band wattmeters for the electrical components. Torque-speed transducers were used to measure the motor shaft output power and axle output shaft power. In addition to the power measurements, average voltage, current and temperature data were recorded. A schematic representation of the propulsion system indicating power measurement locations is shown in Fig. 2.

## Test Description

Transient tests. Prior to running any tests, the proper torque equation coefficients must be established for the vehicle system being characterized. The ETV-1 vehicle parameters relating to tire friction and aerodynamic drag were established from carefully controlled coastdown tests run by Jet Propulsion Laboratory (JPL) (Ref. 3). Using these coastdown curves, coastdown tests were conducted on the RLS and $K_1$, $K_2$, and $K_3$ factors in the torque equation varied until a good match with the JPL results were obtained. The calculated vehicle parameters resulting from these coastdown tests are given in Table 2. With these coefficients, transient tests were run over the SAE J227a B, C, and D driving schedules, at maximum acceleration conditions and at various levels of regenerative braking. All transient tests were performed with Globe-Union EV-2-13 batteries of the type developed under the ETV-1 program.

Steady-state tests. A speed-torque operating envelope for the propulsion system was established by combining data from maximum acceleration and maximum braking tests. This envelope is shown in Fig. 3. Points were distributed within the envelope on lines of constant torque and on the road load torque line. Speeds were chosen on the torque lines to be consistent with the steady speed vehicle tests and others were added to complete the characterization. These test points were used to produce efficiency maps for each component and the system. The two points outside the operating envelope could be obtained because the battery simulator maintains constant voltage independent of current. The operating envelope was originally determined from maximum acceleration data with batteries as the power source and thus includes the effect of a decrease in battery voltage from 108 volts to nearly 85 volts under maximum acceleration. The battery simulator in contrast maintained 105 volts for steady state tests. The notched area in Fig. 3 is discussed under regenerative braking. Steady-state regenerative tests were run at the negative torque conditions indicated on Fig. 3.

## TEST RESULTS

The test results are presented for transient and steady-state tests. Temperature and state-of-charge effects are presented for the steady state tests and energy consumption data for steady state and some transient tests. Transient tests were run with batteries and steady-state tests with the battery simulator.

## Transient Results

Tests were run under conditions of maximum acceleration, various levels of regenerative braking and over SAE J227a B, C, and D driving schedules.

Maximum acceleration. Maximum acceleration tests were conducted using batteries at 0, 40, and 80 percent depth of discharge. These tests were performed by increasing the throttle from zero to full in a two-second period. Since armature current is directly related to throttle position the current goes to its maximum of nearly 400 amps and this level of current is maintained throughout the run. Throttle position was reduced to zero at a vehicle speed of 57 mph. The results of these tests are shown on Fig. 4 where vehicle speed at maximum acceleration is plotted as function of time for the three battery depths of discharge (DOD). It requires 10.5 to 12 seconds to reach 30 mph from rest compared with ETV-1 goal of 9 seconds, the time varying slightly with the battery depth of discharge. Another ETV-1 goal was to accelerate from 25 mph to 55 mph in 18 seconds. This was achieved in 25 seconds for 0 percent and 40 percent discharge and 31 seconds for 80 percent discharge. Power profiles at the battery and at the transaxle output during maximum acceleration are shown on Fig. 5. The battery power increases almost linearly from 0 to 35 kW at 25 mph while the propulsion system is operating in armature control with a current limit. Above 25 mph the power gradually decreases with speed due to a drop in battery voltage.

Regenerative braking. Because of the regenerative braking philosophy incorporated in the design, the portion of the speed-torque plane shown by the hatched area on Fig. 3 is inaccessible. The accelerator and brake pedals in the vehicle each have enable switches that are actuated at the moment either pedal is slightly depressed. When the accelerator is first depressed, the accelerator enable switch closes applying full field voltage to the motor while armature current and consequently motor torque are increased proportional to accelerator position. When the accelerator is returned to zero posi-

tion and there is motor rotation, the vehicle is in the "coast regenerative braking" mode. Actuating the brake switch and depressing the brake increases regenerative braking. In coast, a level of regenerative braking is established to simulate compression braking of an internal combustion engine vehicle coast resulting in a near constant -2500 pound-inch torque at the axle. Regenerative braking increases further in proportion to brake pedal position to -4000 pound-inch maximum. The hatched area in Fig. 3 could be changed by reprogramming the microcomputer.

Transient regenerative braking tests were conducted from a vehicle speed of 50 mph. Results are presented at three conditions - accelerator barely depressed (no armature current commanded but not in coast), coast (accelerator and brake both off), and 100 percent brake. Tests were begun with batteries discharged at least 40 percent. The negative torque portion of Fig. 3, lines 3, 4, and 5, show the speed-torque profile for these three levels of operation. Coast regeneration is approximately 60 percent to 70 percent of the full braking current and consequently 60 percent to 70 percent of the full braking torque. Figure 6 indicates the relationship of armature and battery current as a function of speed with the accelerator slightly depressed, during coast and 100 percent brake. During maximum braking in armature bypass, battery and armature current are nearly equal. In the armature chopper mode, the armature current is maintained near its limit of 200 amps and the resulting battery current decreases. System efficiency relatng to regenerative braking is presented in the steady state results.

SAE J227a driving schedule tests. The SAE J227a B, C, and D driving schedule tests were run for periods of one hour using EV-2-13 batteries as an energy source. The EV-2-13 batteries used for the driving schedule tests had deteriorated and no longer had an adequate capacity. The battery capacity was less than 174 amp hours at the three-hour rate therefore full range tests were not conducted. D schedule data was analyzed and treated in detail in Ref. 4. This data, some new D schedule data, and the B and C schedule data are presented in Table 3. Shown is the energy removed and returned to the battery terminals and axle shaft for the three schedules and the calculated system efficiencies for the motoring portions of the cycle (acceleration and cruise) and for the regenerative portions (coast and brake). A comparison of the D cycle data from Ref. 4 showed a net energy difference of 10 percent higher than that in Ref. 3. This led to some additional D cycle tests on the RLS where the coast and brake profiles were changed, i.e. the coast and brake profile was adjusted to more closely approximate the deceleration of an internal combustion engine vehicle. This revised (partial coast) "D" cycle profile resulted in reduced deceleration rates and less energy being regenerated during coast and brake. This results in a higher net energy per cycle and a lower percent energy returned to the battery. Both sets of results are presented in Table 3 for comparison.

Steady-State Results

The primary goal of the steady-state testing was system characterization. Consistent with this goal, test conditions were set and results reported on a basis of vehicle speed and transaxle output torque. Component and system efficiencies vary with battery voltage and the component temperatures. Data were obtained over a range of temperatures and voltage, but the data presented in Figs. 7 to 11 are for a fixed voltage of 105 volts and a motor temperature of 110° F. The effects of voltage and temperature variations are indicated in Figs. 12 and 13.

Efficiency calculations. The efficiency of each component was calculated using the data from six power measurements (Fig. 2) and applying the basic equation $\eta = P_{out}/P_{in}$,

where

$\eta$ - Efficiency
$P_{out}$ - Power output
$P_{in}$ - Power input

The accessory power (PACSY) was found to be nearly constant and independent of operating conditions. It was also found that the accessory charger interfered with other electrical power measurements so it was made inoperative for most all of the tests. A constant accessory power was assumed in all system calculations.
A fully charged accessory battery was installed at the beginning of each test. The component efficiencies were calculated as follows: motor input power, PMOT, is calculated by adding armature power and field power. Then from the efficiency equaton:

$$\text{controller} \quad \eta = \frac{PMOT}{PBAT}$$

$$\text{motor} \quad \eta = \frac{HPMOT}{PMOT}$$

$$\text{transaxle} \quad \eta = \frac{HPTAXL}{HPMOT}$$

$$\text{system} \quad \eta = \frac{HPTAXL}{PBAT + PACSY}$$

where symbols are defined in Fig. 2.

Regenerative braking efficiencies are calculated from the inverse of these equations.

Efficiency results, motoring mode. The efficiency is plotted as a function of output torque and vehicle speed. Efficiencies are presented for lines of constant torque and for the road load torque line. System efficiency and motor efficiency are shown on Figs. 7 and 8, respectively. The shapes

of these curves are very similar as the system efficiency is dominated by the motor characteristics. Note in both figures that an inflection occurs from 20-25 mph in the armature chopper control region. This inflection is believed to be caused by the effect of the chopper waveform on the harmonic motor losses.

The controller efficiency at all operating conditions tested was above 80 percent. It is shown as a function of speed in the form of an envelope on Fig. 9. The lowest measured efficiency, occurring at 4000 pound-inches and 5 mph, is 82 percent. Efficiency in armature bypass at all conditions is in excess of 95 percent. The controller losses during armature bypass are composed of the logic power supply, field chopper and contactors which are very low relative to the power output at high power conditions.

Transaxle efficiency shown in Fig. 10 is above 96 percent at the higher torque levels. Fixed torque losses at lower power levels, typical of mechanical transmissions, account for the reduction in efficiency on the road load torque line.

Efficiency results, regenerative mode. The component and system efficiencies for regenerative braking are shown in Fig. 11. Higher regenerative efficiency is obtained in the armature bypass mode (as the motor armature is directly across the battery) than in the armature chopper mode. The armature chopper is used below motor base speed to boost the armature voltage above battery voltage. A net power flow to the batteries is obtained above 5 mph.

## Temperature-State-of-Charge Effects

The transaxle is sensitive to temperature, and the electrical components to voltage (state of charge) and temperature. Motor efficiency is the most sensitive to these effects.

Temperature effects. Motor temperature was sensed by four thermocouples, two at each end of the field windings. The four temperatures were averaged and the average used as the representative temperature in the data presented. In general, the brush end of the motor was significantly hotter when operating in the armature chopper mode than when in bypass. Motor efficiency is plotted in Fig. 12 as a function of average motor temperature for three different battery voltages at 45 mph and road load torque. Motor efficiency at this speed torque condition increases as temperature and voltage increase. At other torque speed conditions, different trends were experienced and are discussed with state-of-charge effects. These will be presented in a NASA report (Ref. 5) to be published soon.

The controller was instrumented with four thermocouples - one on the armature chopper transistor heat sink, one on the regenerative chopper transistor heat sink, one in air near the logic power supply, and one in air near the accessory charger. While the efficiency of the controller varies with operating time implying that it varies with temperature, no representative temperature exists to which the efficiency change can be related. The heat sink casting which cools the power transistors rarely exceeds 120° F. The logic power supply and accessory charger temperatures stabilized near 140° F independent of operating condition.

Transaxle oil temperature is measured by a pair of redundant thermocouples submerged in the oil and entering through the oil drain plug. The two measurements were averaged. Transaxle efficiency always increases with increasing temperature. Transaxle efficiency versus temperature is shown in Fig. 13 for two long term tests. The hottest temperature (155° F) occurred at the end of a 45 mph, 788 pound-inch test but had not yet stabilized after one and a half hours. Efficiency varied from 90.5 percent to 92 percent over the duration of the test.

State-of-charge effect. The effect of voltage (due to battery state of charge) on the motor efficiency is as significant as the temperature effect. The voltage effect can be positive or negative depending on operating conditions. Referring again to Fig. 12 motor efficiency increases as battery voltage increases at this particular high speed low torque condition. Below motor base speed (armature chopper mode) the motor efficiency decreases with increasing battery voltage and increasing temperature. Above motor base speed, motor efficiency increases with increasing battery voltages and increases with higher temperature at low torque (low current) but decreases at high torques (high current) Ref. 5.

The voltage effect on the controller is less than 2 percent for any speed-torque point. The major effect occurs just before armature chopper bypass (25 mph) and also at the high power levels. The controller efficiency decreases with increasing battery voltage at low power levels and begins to increase as power level increases.

It appears that the performance of the controller and motor are related. This is confirmed in Ref. 6 where chopper controllers are shown to reduce motor efficiency.

Energy consumption. Energy consumption was calculated from the power measurements for steady speeds of 25, 35, 45 and 55 mph and the SAE J227a driving schedules B, C, and D. For the steady speed tests, energy consumption was computed by dividing the battery power by the vehicle speed. For the driving schedules, battery power was integrated over time yielding net energy per cycle and divided by the distance traveled per cycle. Results for five of these test conditions were also reported by JPL for the ETV-1 vehicle in Ref. 3. NASA LeRC, the JPL results and the GE computer model predictions (Ref. 5) are compared in Fig. 14. No comparative data were available for the B and C driving schedules.

The agreement between the JPL vehicle dynamometer tests and the NASA-LeRC RLS tests are within 6 percent in all cases. In the 45 mph and 55 mph cases where the

results differ by 5 percent and 6 percent, the variations are due to differences in the road loads at which the tests were run. This excellent agreement adds verification that the breadboard is a truly representative configuration of the vehicle propulsion system.

## CONCLUDING REMARKS

The ETV-1 breadboard propulsion system has been characterized under steady-state conditions throughout its motoring and regenerating operating regimes. In addition, test data were obtained under conditions of maximum acceleration, maximum braking and the SAE J227a B, C, and D driving schedules. No areas of propulsion system instability were found during these tests. One area was discovered in the regenerative regime where operation could not be achieved. This area was created by design to provide a fixed amount of regenerative braking during coast. Re-evaluation of the size of this excluded speed-torque area (refer to Fig. 3) would be worthwhile.

Excellent agreement was obtained between tne ETV-1 vehicle dynamometer test data obtained by JPL and the ETV-1 breadboard test data obtained on the Road Load Simulator. The breadboard concept for detailed propulsion system evaluation on the Road Load Simulator has shown itself to be a valuable tool to aid in electric vehicle research.

## REFERENCES


1 Wilson, J. W. A., "The Drive System of the DOE Near-Term Electric Vehicle (ETV-1)," SAE Paper 800058, Feb. 1980.

2 Sargent, N. B., "A Laboratory Facility for Electric Vehicle Propulsion System Testing," DOE/NASA 11011-32, NASA TM-81574, Sep. 1980.

3 Kurtz, D. W., Price, T. W., and Bryant, J. A., "Performance Testing and System Evaluation of the DOE ETV-1 Electric Vehicle," SAE Paper 810418, Feb. 1981.

4 Sargent, N. B., and Dustin, M. O., "Characterization of the Near-Term Electric Vehicle (ETV-1) Breadboard Propulsion System Over the SAE J227a Driving Schedule D, DOE/NASA 51044-15, NASA TM-81664, Feb. 1981.

5 NASA Steady State Report in Progress.

6 Schwab, J. R., "Performance of a 14.9 kW Laminated-Frame dc Series Motor with Chopper Controller," DOE/NASA 104479/2, NASA TM-79177, June 1979.


TABLE I - ETV-1 COMPONENT SPECIFICATIONS

Motor

Type - dc shunt, force ventilated
Power rating - 15 kW, continuous
Voltage - 108V
Maximum speed - 5,000 rpm

Controller

Type - Transistorized, armature chopper, field chopper, microprocessor controlled
Maximum current - 400 amps motoring, 200 amps regenerative braking
Cooling - Forced air

Speed Reducer and Differential

Type - 2-stage chain reduction
Ratio - 5.48
Differential - Omni/Horizon, modified

Batteries

Type - Globe-Union EV-2-13, lead-acid
Voltage - 108 volts (18 - 6V modules)
Weight - 1,092 pounds
Capacity - 174 amp-hours (3 hr rate)

TABLE 2 - VEHICLE PARAMETERS

Tire friction* - 0.0095 pounds/pound
Aerodynamic losses, $C_dA$* - 6.4 $ft^2$
Vehicle weight - 3900 pounds
Rolling radius - 0.921 ft

*Experimentally determined

TABLE 3 - SUMMARY OF DRIVING SCHEDULE TEST ENERGY DATA*

| | Schedule B | Schedule C | Partial "coast" Schedule D | Full "coast" Schedule D |
|---|---|---|---|---|
| $E_B$, out (acceleration and cruise) | 65 wh | 101 wh | 286 wh | 280 wh |
| $E_B$, in (coast and brake) | 4.3 wh | 13 wh | 43 wh | 54 wh |
| $E_T$, out (acceleration and cruise) | 35 wh | 68 wh | 213 wh | 212 wh |
| $E_T$, in (coast and brake) | 9.9 wh | 24 wh | 57 wh | 71 wh |
| $\eta_s$, out = $\frac{E_T, \text{ out}}{E_B, \text{ out}}$ (motoring) | 54 percent | 67 percent | 74 percent | 75.7 percent |
| $\eta_s$, in = $\frac{E_B, \text{ in}}{E_T, \text{ in}}$ (regen. braking) | 43 percent | 54 percent | 75 percent | 76.1 percent |
| Percent energy returned to battery = $\frac{E_B, \text{ in}}{E_B, \text{ out}}$ | 6.6 percent | 13 percent | 15 percent | 19.3 percent |
| Distance traveled per cycle | 0.19 mi | 0.33 mi | 0.98 mi | 0.99 mi |
| where: | | | | |
| $E_B$ - Energy at battery terminals | | | | |
| $E_T$ - Energy at axle shaft | | | | |
| $\eta_s$ - System efficiency | | | | |

*Energy data in watthours per driving cycle

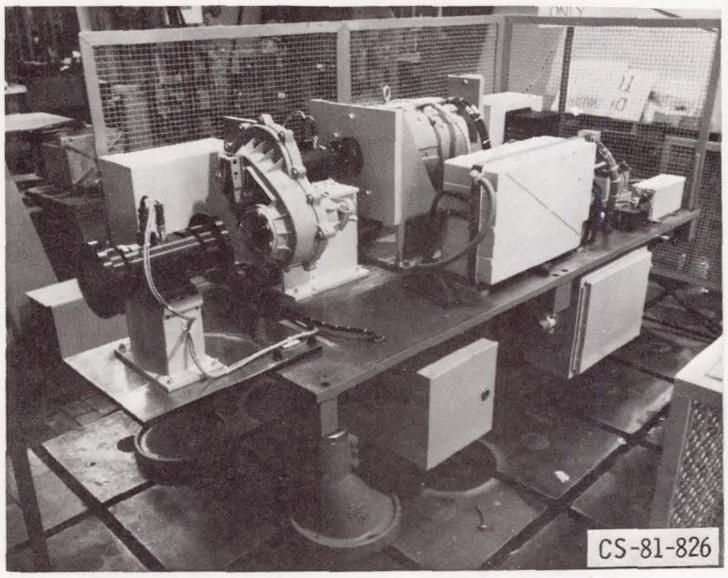


Figure 1. - ETV-1 propulsion system breadboard.

PBAT - BATTERY POWER
PACSY - ACCESSORY POWER
PARM - ARMATURE POWER
PFLD - FIELD POWER
HPMOT - MOTOR SHAFT POWER
HPTAXL - AXLE SHAFT POWER

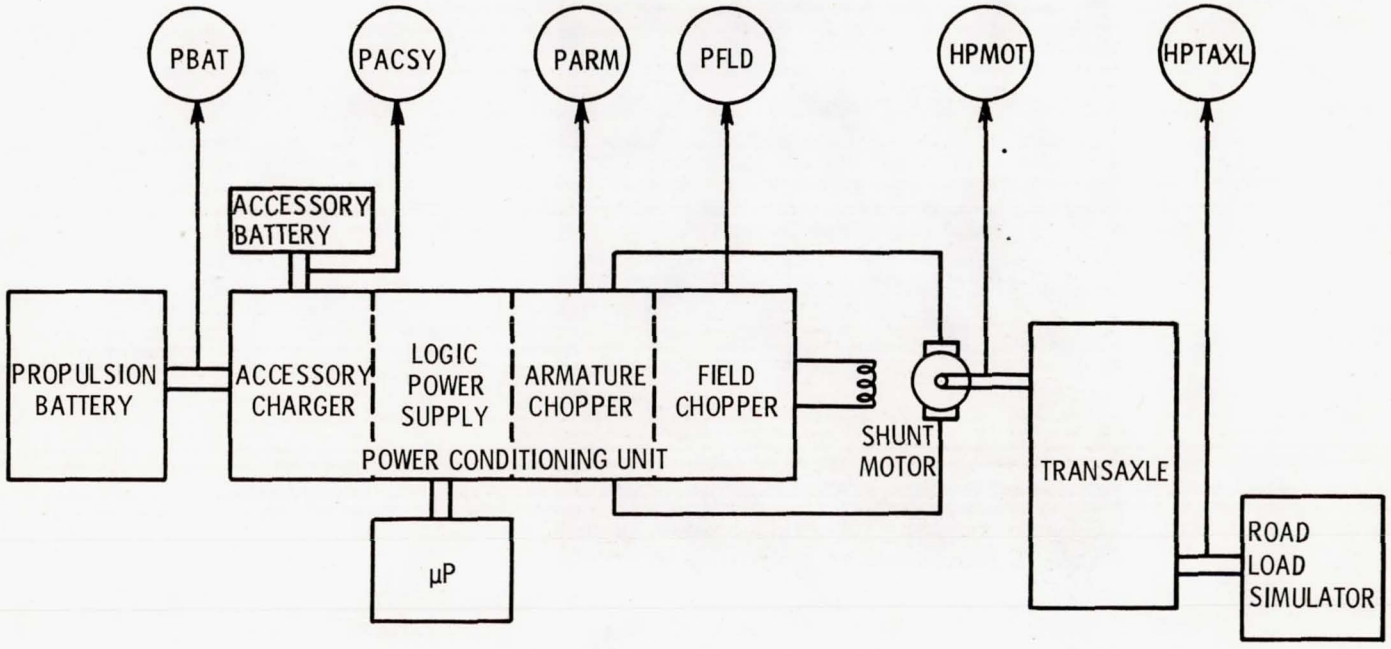


Figure 2. - Power flow measurement block diagram.

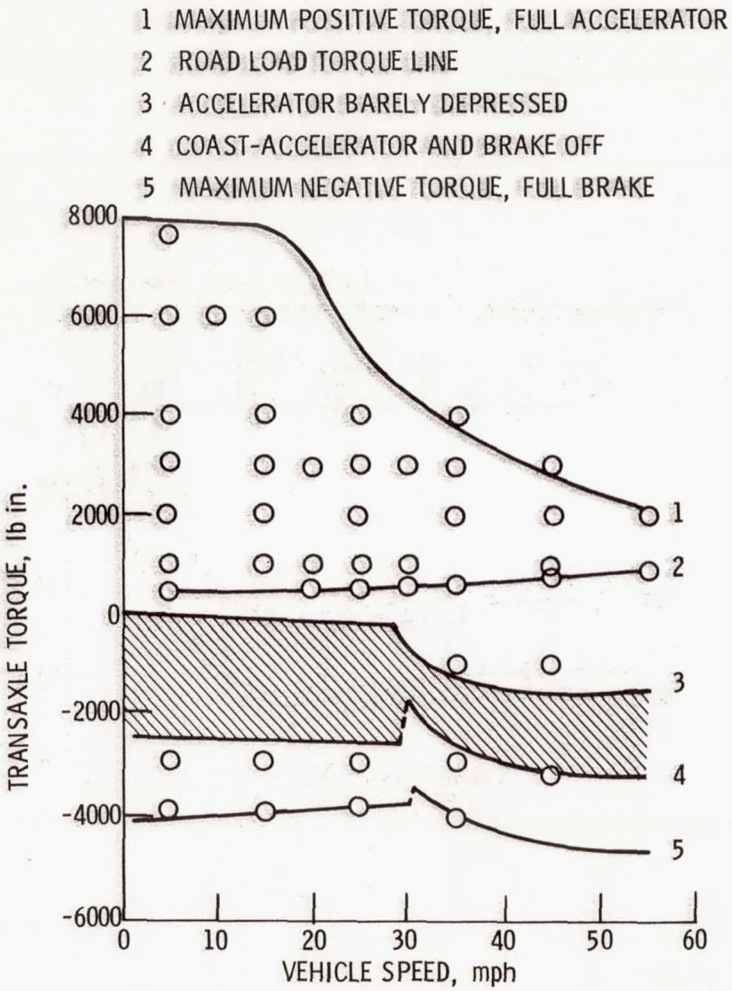


Figure 3. - Speed-torque operating envelope with steady-state test points.

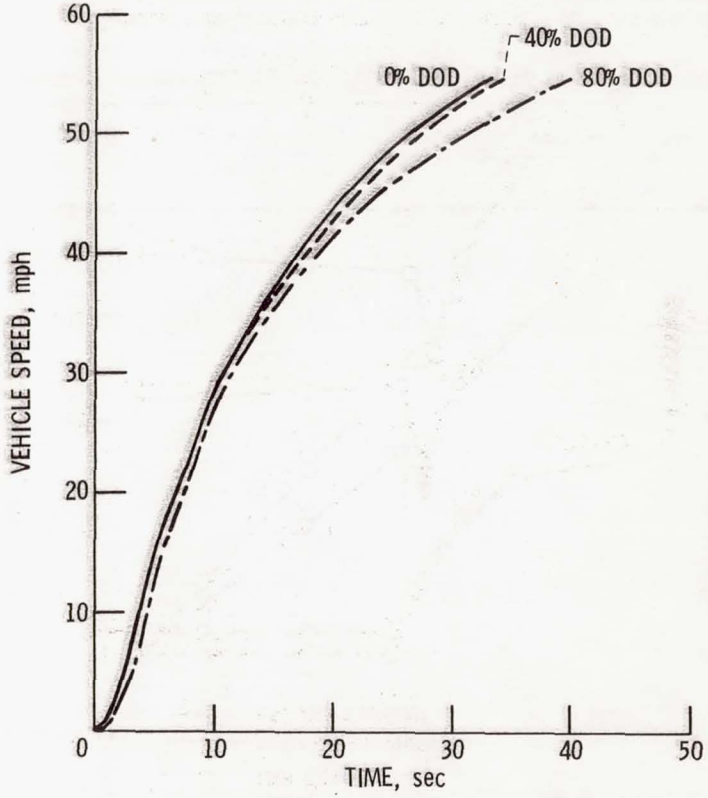


Figure 4. - Vehicle speed as a function of time under maximum acceleration at 3 depths of discharge (DOD).

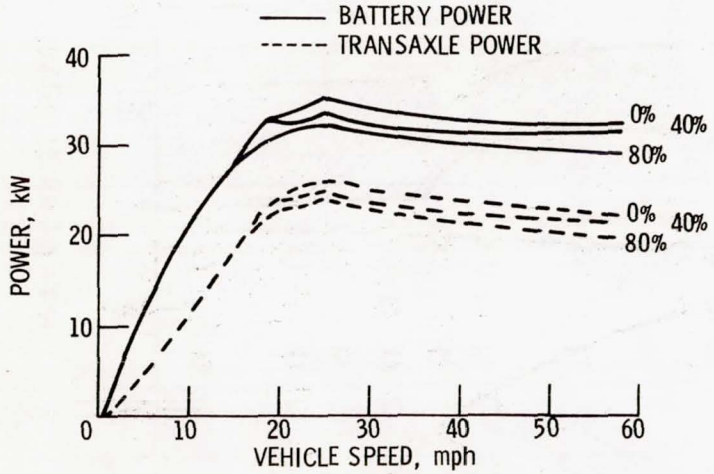


Figure 5. - Input and output power as a function of vehicle speed under maximum acceleration.

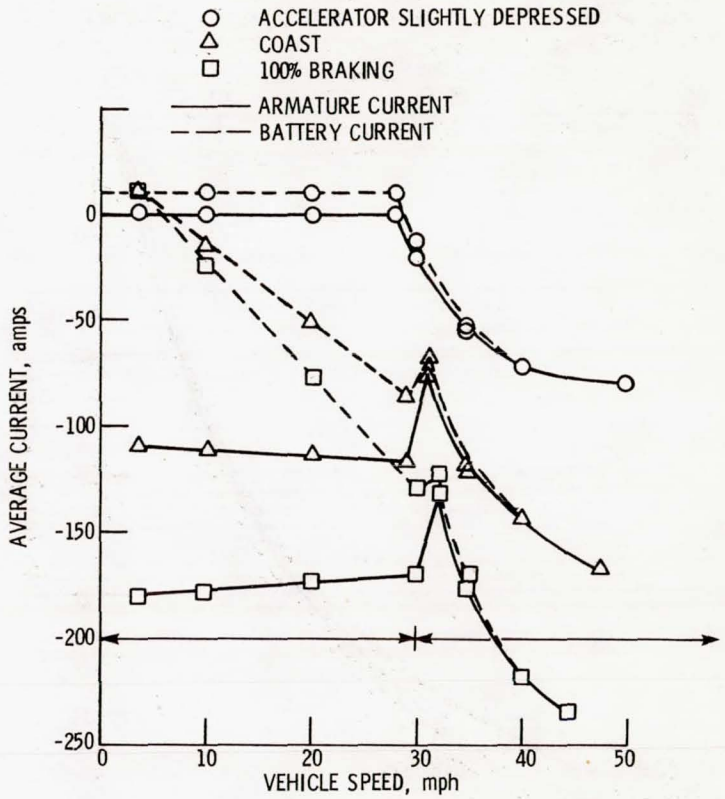


Figure 6. - Regenerative current as a function of vehicle speed.

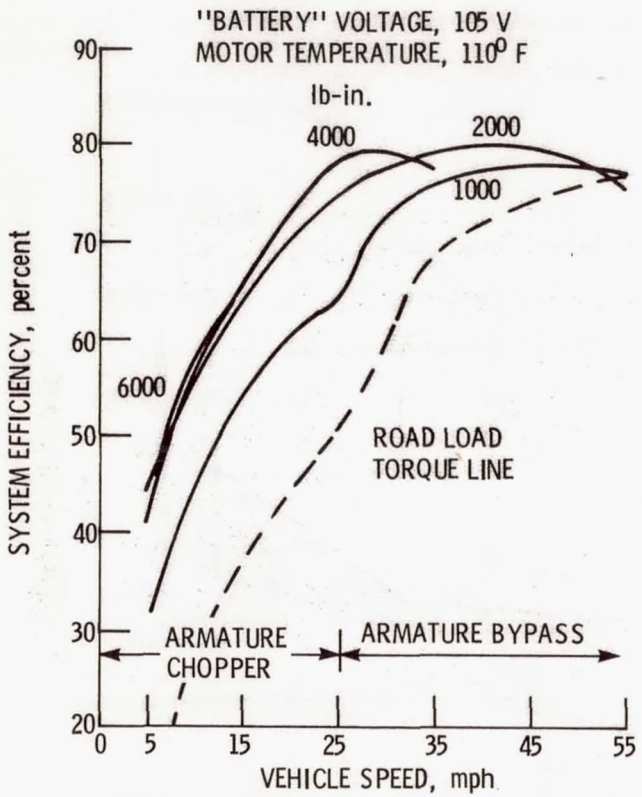


Figure 7. - System efficiency as a function of vehicle speed on lines of constant transaxle torque (lb-in. ).

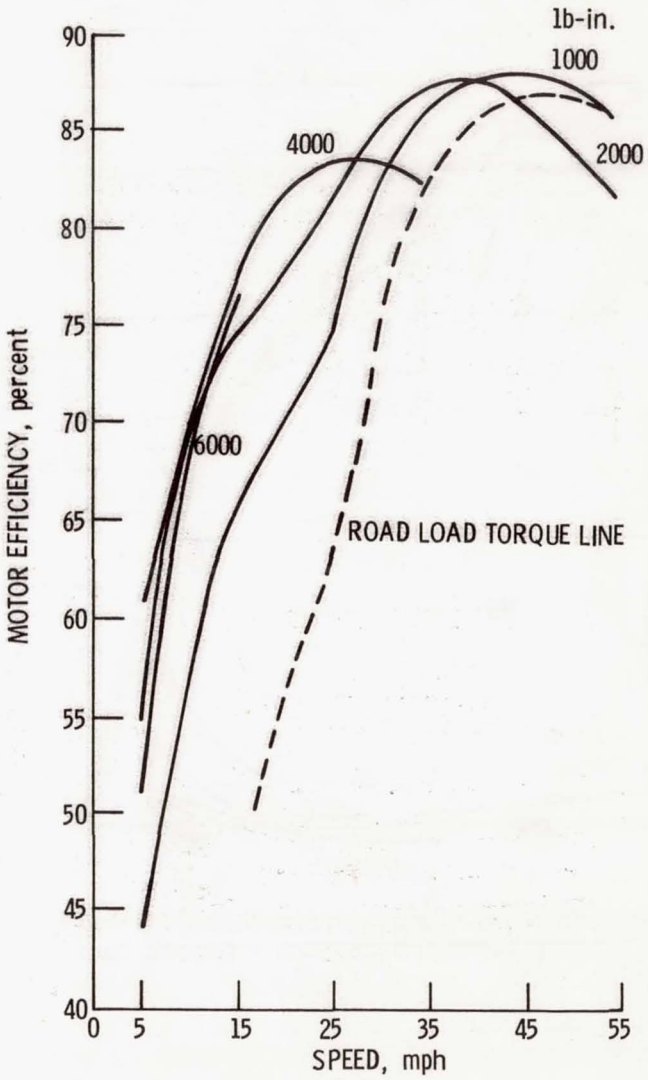


Figure 8. - Motor efficiency as a function of vehicle speed on lines of constant transaxle torque.

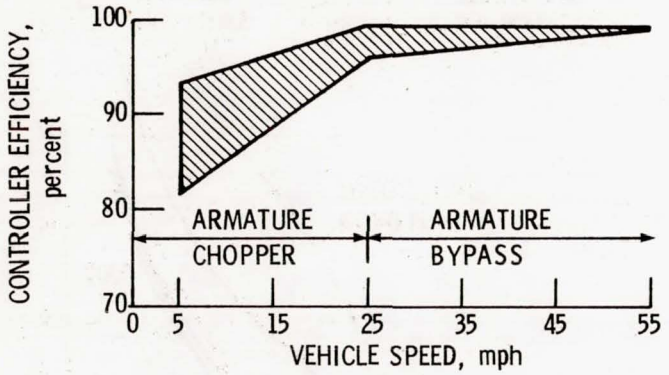


Figure 9. - Controller efficiency envelope as a function of vehicle speed.

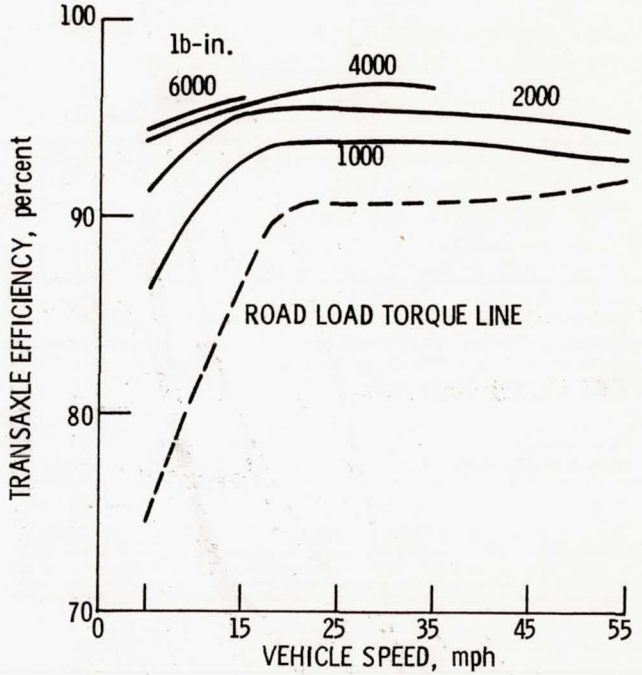


Figure 10. - Transaxle efficiency speed on lines of constant transaxle torque.

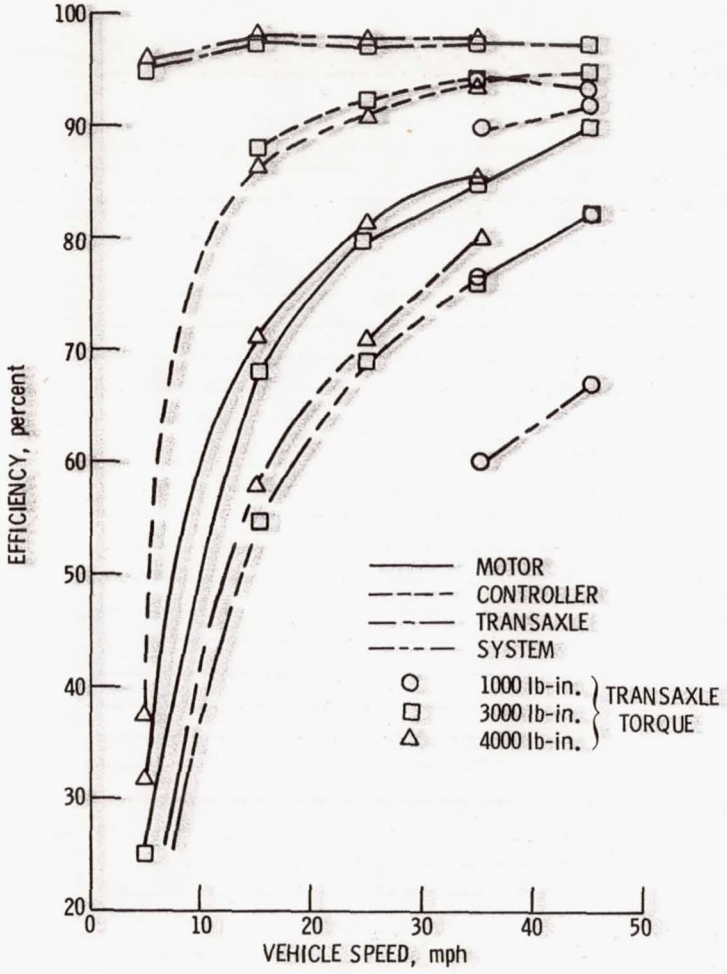


Figure 11. - Regenerative braking efficiencies as a function of vehicle speed.

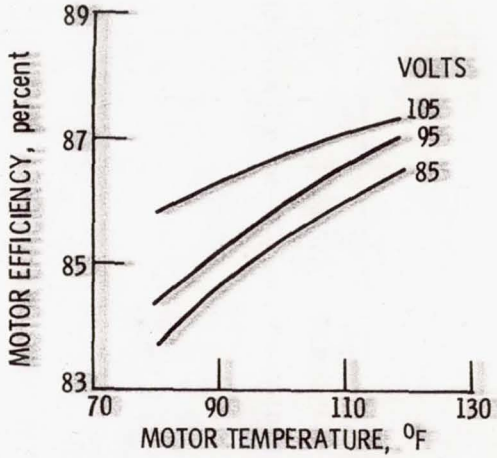


Figure 12. - Motor efficiency as a function of temperature at 45 mph and 788 lb-in. at 3 battery simulator voltages.

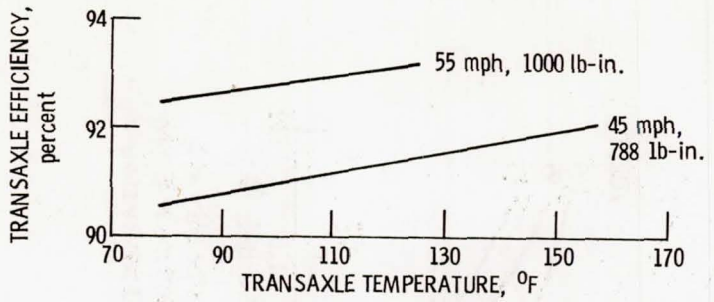


Figure 13. - Transaxle efficiency as a function of temperature.

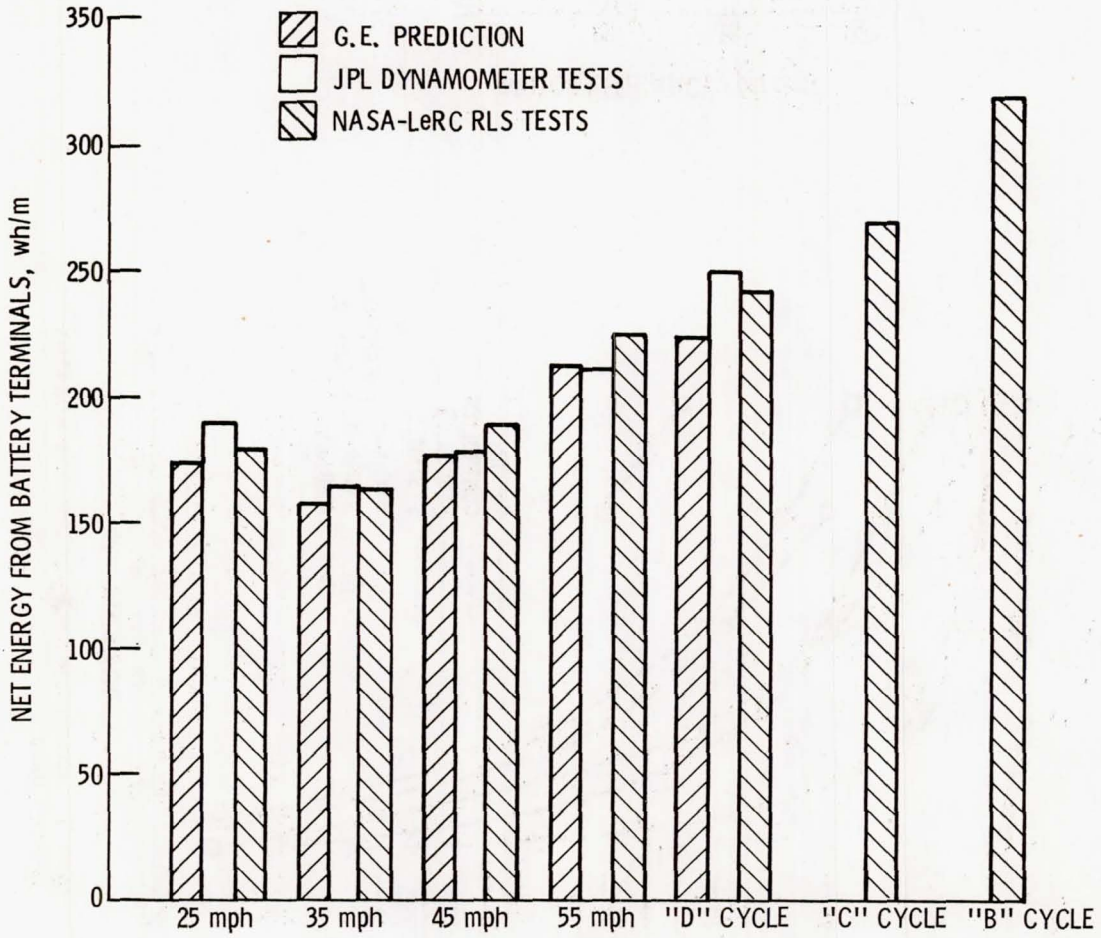


Figure 14.

| 1. Report No. NASA TM-82667 | 2. Government Accession No. | 3. Recipient's Catalog No. |
|---|---|---|
| 4. Title and Subtitle RESULTS OF THE ETV-1 BREADBOARD TESTS UNDER STEADY-STATE AND TRANSIENT CONDITIONS | | 5. Report Date August 1981<br>6. Performing Organization Code 778-36-06 |
| 7. Author(s) Noel B. Sargent and Miles O. Dustin | | 8. Performing Organization Report No. E-944<br>10. Work Unit No. |
| 9. Performing Organization Name and Address National Aeronautics and Space Administration Lewis Research Center Cleveland, Ohio 44135 | | 11. Contract or Grant No. |
| 12. Sponsoring Agency Name and Address U.S. Department of Energy Office of Vehicle and Engine R&D Washington, D.C. 20545 | | 13. Type of Report and Period Covered Technical Memorandum<br>14. Sponsoring Agency Code DOE/NASA/51044-21 |

15. Supplementary Notes

Prepared under Interagency Agreement DE-AI01-77CS51044. Prepared for Electric Vehicle Council Symposium VI, Baltimore, Maryland, October 21-23, 1981.

16. Abstract

This paper presents the test results of a breadboard version of the ETV-1 electric vehicle propulsion system built by General Electric Company under contract to NASA-LeRC as a part of the Department of Energy (DOE) Electric and Hybrid Vehicle Program. The breadboard was installed in the NASA-LeRC Road Load Simulator facility and tested under steady state and transient conditions. Steady state tests were run to characterize the system and component efficiencies over the complete speed-torque capabilities of the propulsion system in both motoring and regenerative modes of operation. The steady state data were obtained using a battery simulator to separate the effects on efficiency caused by changing battery state-of-charge and component temperature. Transient tests were performed to determine the energy profiles of the propulsion system operating over the SAE J227a driving schedules.

| 17. Key Words (Suggested by Author(s)) | 18. Distribution Statement |
|---|---|
| Electric propulsion<br>Batteries<br>Automotive | Unclassified - unlimited<br>STAR Category 44<br>DOE Category UC-96 |

| 19. Security Classif. (of this report) | 20. Security Classif. (of this page) | 21. No. of Pages | 22. Price* |
|---|---|---|---|
| Unclassified | Unclassified | | |

* For sale by the National Technical Information Service, Springfield, Virginia 22161